

Supporting Information

Supramolecular Polymerization of Electronically Complementary Linear Motifs: Anti-Cooperativity by Attenuated Growth

Yeray Dorca,^{†a} Cristina Naranjo,^{†a} Goutam Ghosh,^b Bartolomé Soberats,^c Joaquín Calbo,^d Enrique Ortí,^{*d} Gustavo Fernández,^{*b} and Luis Sánchez^{*a}

Table of Contents

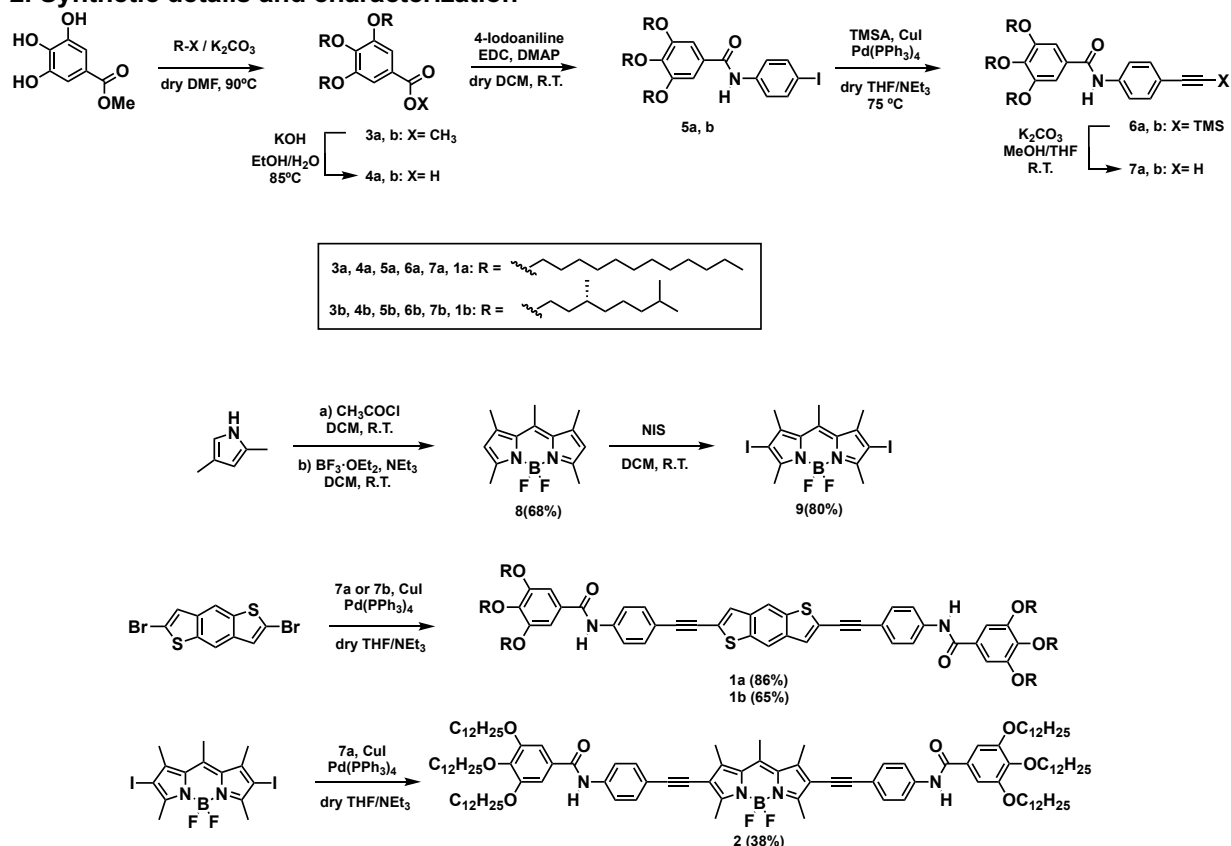
1. <i>Experimental section</i>	S-2
2. <i>Synthetic details and characterization</i>	S-2
3. <i>Collection of spectra</i>	S-4
4.- <i>Supplementary Figures</i>	S-7
<i>UV-Vis studies for BDT-based 1</i>	S-7
<i>FTIR spectra in solution of 1 and 2</i>	S-7
<i>Dimensions of the BDT and BODIPY cores</i>	S-8
<i>AFM images of pristine 1a, 1b and 2</i>	S-9
<i>SAXS of pristine 1a, 1b and 2</i>	S-9
<i>Optimized geometries for 1 and 2</i>	S-10
<i>VT-UV-Vis and emission experiments for 1-co-2</i>	S-14
<i>CD experiments for 1b and 1b-co-2</i>	S-15
<i>SAXS of 1a-co-2 and 1b-co-2</i>	S-16
<i>AFM images of 1a-co-2</i>	S-16
5. <i>SAXS measurements</i>	S-17
6. <i>Theoretical calculations</i>	S-17
7. <i>References</i>	S-17

Experimental Procedures

General. All solvents were dried according to standard procedures. Reagents were used as purchased. All air-sensitive reactions were carried out under argon atmosphere. Flash chromatography was performed using silica gel (Merck, Kieselgel 60, 230–240 mesh or Scharlau 60, 230–240 mesh). Analytical thin layer chromatography (TLC) was performed using aluminium-coated Merck Kieselgel 60 F254 plates. NMR spectra were recorded on a Bruker Avance 500 (^1H : 500 MHz; ^{13}C : 125 MHz) spectrometer at 298 K using partially deuterated solvents as internal standards. Coupling constants (J) are denoted in Hz and chemical shifts (δ) in ppm. Multiplicities are denoted as follows: s = singlet, d = doublet, t = triplet, m = multiplet, br = broad. FTIR spectra were recorded on a JASCO-FT-IR-6800 spectrometer using a CaF_2 cell with a path length of 0.1 mm. High-resolution mass spectra (HRMS) were recorded on a FTMS Bruker APEX Q IV spectrometer. UV-Vis spectra were recorded on a JASCO V-630/750 spectrophotometer by using quartz cuvettes (Hellma). Thermal experiments were performed at constant cooling rates of 1 K min^{-1} from 293 to 363 K in methylcyclohexane (MCH). PL emission spectra were recorded on a JASCO FP-8500 spectrofluorometer. Circular dichroism (CD) measurements were performed on a JASCO-1500 dichrograph equipped with a Peltier thermoelectric temperature controller. The spectra were recorded in the continuous mode between 220 and 600 nm, with a wavelength increment of 0.2 nm, a response time of 1 s, and a bandwidth of 2 nm using a quartz cuvette (Hellma). Atomic force microscopy (AFM) was performed on a SPM Nanoscope IIIa multimode microscope working on tapping mode with a RTESPA tip (Veeco) at a working frequency of $\sim 235 \text{ kHz}$. Small angle X-ray scattering (SAXS) measurements were performed on a XENOCES XEUS 3.0. The instrument is equipped with a GeniX 3D Cu micro focus X-ray source ($\lambda = 1.54 \text{ \AA}$; flux = $2 \times 10^8 \text{ ph s}^{-1}$) and a DECTRIS Pilatus3 R 300K silicon pixel detector with 487×619 pixels of $172 \times 172 \mu\text{m}$ in size. Experiments were performed with a sample-to-detector distance of 500 mm to access a q -range of $0.007 \leq q \leq 0.57 \text{ \AA}^{-1}$ ($q = 4\pi/\lambda (\sin\theta/2)$). All the samples were measured in 2 mm glass capillaries (Capillary Tubes Supplies Ltd., UK). Measurement times were in between 2400 and 3600 seconds.

Preparation of solutions for spectroscopic measurements. Stock solutions (1 mM) in CHCl_3 were prepared by weighing the appropriate amount of compound that it is subsequently dissolved by adding the corresponding volume of CHCl_3 . The stock solutions were sonicated for 1 minute and heated up to $40 \text{ }^\circ\text{C}$ in a water bath until solid material was completely dissolved. The solutions of compounds **1** or **2** in MCH were prepared by aliquoting the desired volume of the stock solution in CHCl_3 in a vial. The CHCl_3 was eliminated by blow-drying and the appropriate volume of MCH added. The resulting MCH solution, in which no precipitate is observed, is heated up to $90 \text{ }^\circ\text{C}$ for 30 minutes and cooled down to $20 \text{ }^\circ\text{C}$ prior to the corresponding measurement.

2. Synthetic details and characterization



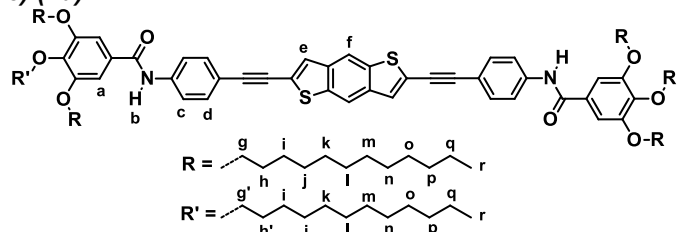
Scheme S1. Synthesis of the reported BDT (**1a,b**) and BODIPY (**2**) derivatives.

Compounds **2–9**,^{S1} were prepared according to previously reported synthetic procedures and showed identical spectroscopic properties to those reported therein.

Synthesis of the BDT derivatives 1a and 1b. General procedure.

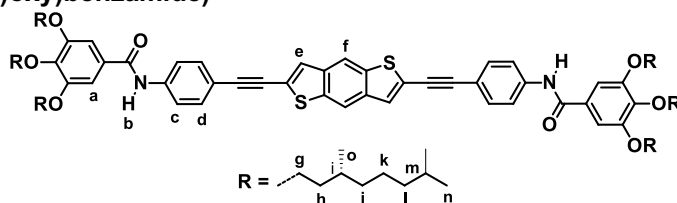
Commercially available 2,6-dibromobenzo[1,2-b:4,5-b']dithiophene (42 mg, 0.12 mmol), tetrakis(triphenylphosphine)palladium(0) (7 mg, 6 μ mol) and CuI (1.1 mg, 6 μ mol) were weighed in a 100 mL Schlenk flask. After 4 vacuum-nitrogen cycles, dry NEt_3 (5 mL) was added to the flask and 2 additional vacuum-nitrogen cycles were done. After that, alkyne **7a** or **7b** (0.26 mmol) was separately dissolved in dry THF (20 mL) and added dropwise. The reaction mixture was stirred at 70 °C for 24 h. After evaporation of the solvent under reduced pressure, the residue was purified by column chromatography (silica gel, CH_2Cl_2 as eluent).

N,N'-((benzo[1,2-b:4,5-b']dithiophene-2,6-diylbis(ethyne-2,1-diyl))bis(4,1-phenylene))bis(3,4,5-tris(dodecyloxy)benzamide) (**1a**).



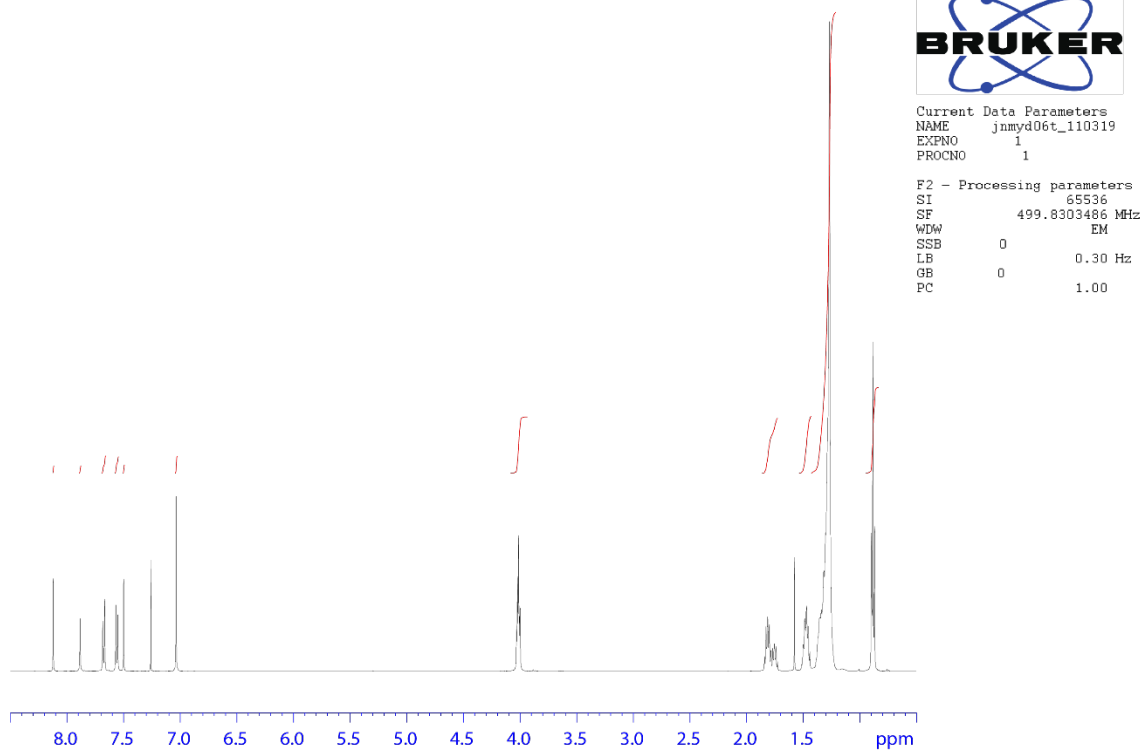
The title compound **1a** (180 mg, 86%) was isolated as a yellow solid. ^1H NMR (CDCl_3 , 500 MHz) δ (ppm) 8.13 (s, 2H, H_f), 7.90 (s, 2H, H_b), 7.68 (d, $^3J = 8.49$ Hz, 4H, H_c), 7.56 (d, $^3J = 8.49$ Hz, 4H, H_d), 7.51 (s, 2H, H_e), 7.04 (s, 4H, H_a), 4.02 (m, 12H, $\text{H}_{g,g'}$), 1.82 (m, 8H, $\text{H}_{h,h'}$), 1.76 (m, 4H, H_i), 1.48, (m, 12H, H_j), 1.27 (br, 96H, H_{k-q}), 0.89 (t, $^3J = 6.3$ Hz, 18H, H_r). ^{13}C NMR (CDCl_3 , 125 MHz) δ 165.64, 153.27, 141.75, 138.59, 137.85, 137.77, 132.52, 129.52, 127.61, 124.22, 119.80, 118.14, 116.39, 105.85, 95.54, 82.96, 73.58, 69.49, 31.94, 31.93, 30.34, 29.77, 29.76, 29.75, 29.74, 29.71, 29.70, 29.67, 29.65, 29.59, 29.42, 29.39, 29.37, 26.09, 22.70, 22.69, 14.11. FT-IR (ν / cm^{-1}) = 3272, 2919, 2851, 1647, 1580, 1539, 1505, 1493, 1467, 1426, 1403, 13337, 1292, 1238, 1169, 1117, 1065, 999, 855, 828, 790, 720. HR-MS-MALDI-TOF m/z : $\text{C}_{112}\text{H}_{168}\text{N}_2\text{O}_8\text{S}_2$ $[\text{M}]^+$ calculated, 1733.2242; $[\text{M}]^+$ found, 1733.2320.

(*R,R,R*)-*N,N'*-((benzo[1,2-b:4,5-b']dithiophene-2,6-diylbis(ethyne-2,1-diyl))bis(4,1-phenylene))bis(3,4,5-tris(((*R*)-3,7-dimethyloctyl)oxy)benzamide)

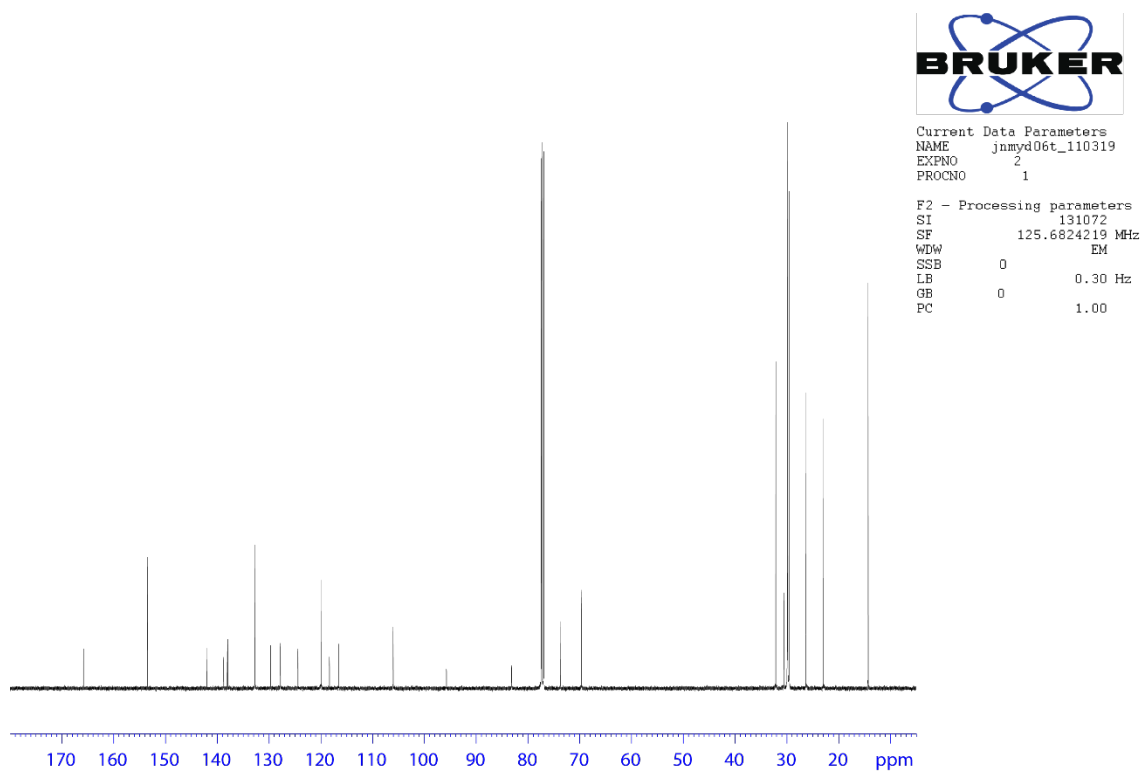


The title compound **1b** (176 mg, 65%) was isolated as a yellow solid. ^1H NMR (CDCl_3 , 500 MHz) δ 8.14 (s, 2H, H_f), 7.80 (s, 2H, H_b), 7.68 (d, $^3J = 8.5$ Hz, 4H, H_c), 7.58 (d, $^3J = 8.49$ Hz, 4H, H_d), 7.51 (s, 2H, H_e), 7.06 (s, 4H, H_a), 4.07 (m, 12H, H_g), 1.86-1.72 (m, 18H, $\text{H}_{h,i}$), 1.53-1.16, (m, 42H, $\text{H}_{j,k,l,m}$), 0.94 (m, 18H, H_o), 0.87 (d, $^3J = 6.3$ Hz, 36H, H_n). ^{13}C NMR (CDCl_3 , 125 MHz) δ 153.4, 141.9, 138.8, 138.2, 132.7, 129.8, 127.7, 119.9, 116.5, 105.9, 83.2, 71.7, 67.9, 39.5, 39.4, 37.6, 36.4, 36.5, 29.9, 29.8, 29.7, 28.1, 24.8, 22.8, 22.7, 19.7. FT-IR (ν / cm^{-1}) = 3277, 2921, 2852, 1716, 1635, 1605, 1586, 1555, 1496, 1466, 1429, 1390, 1334, 1263, 1204, 1113, 1061, 1007, 907, 848, 763, 728. HR-MS-MALDI-TOF m/z : $\text{C}_{100}\text{H}_{144}\text{N}_2\text{O}_8\text{S}_2$ $[\text{M}+\text{H}]^+$ calculated, 1566.0364; found, 1566.0441.

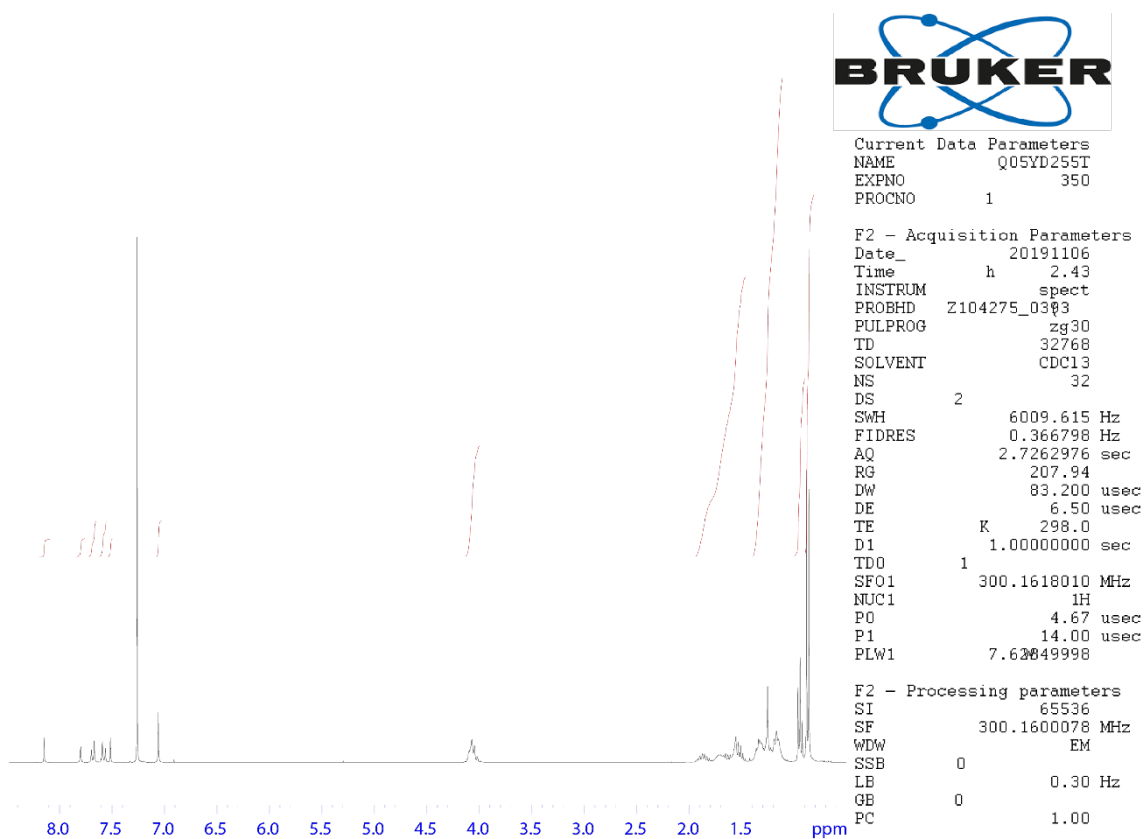
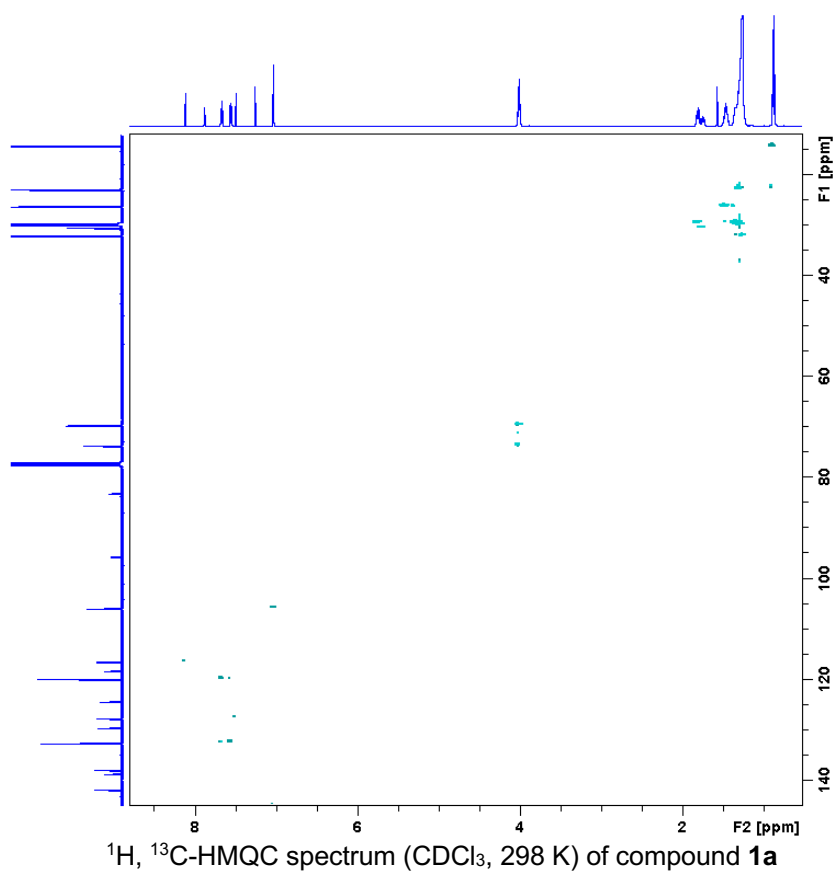
3. Collection of spectra



¹H NMR (CDCl₃, 500 MHz, 298 K) of compound **1a**



¹³C NMR (CDCl₃, 125 MHz, 298 K) of compound **1a**



Current Data Parameters
 NAME Q05YD255T
 EXPNO 350
 PROCNO 1

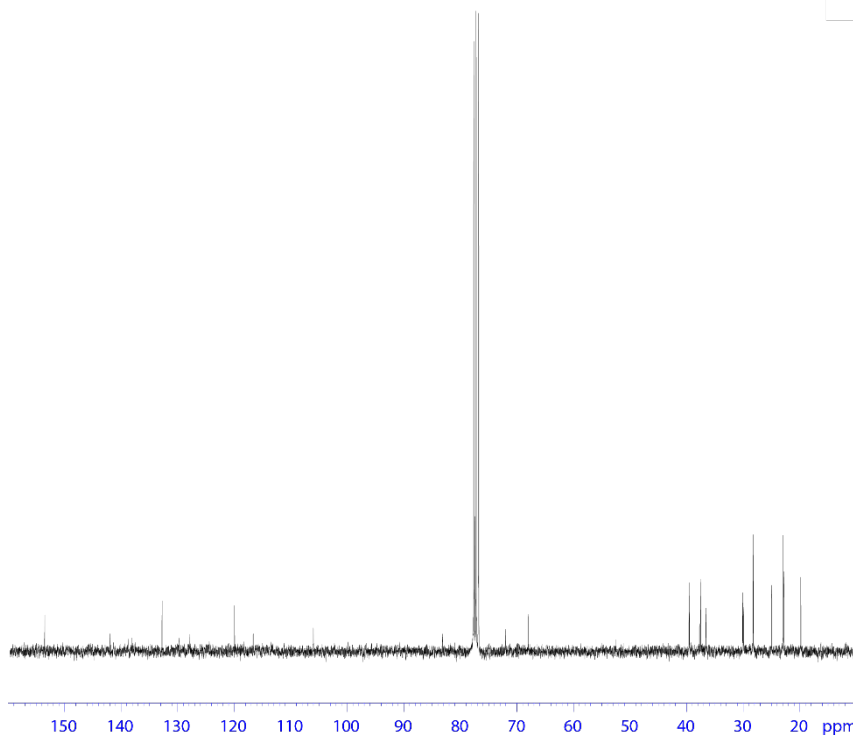
F2 - Acquisition Parameters
 Date_ 20191106
 Time h 2.43
 INSTRUM spect
 PROBHD Z104275_0303
 PULPROG zg30
 TD 32768
 SOLVENT CDCl_3
 NS 32
 DS 2
 SWH 6009.615 Hz
 FIDRES 0.366798 Hz
 AQ 2.7262976 sec
 RG 207.94
 DW 83.200 usec
 DE 6.50 usec
 TE K 298.0
 D1 1.00000000 sec
 TDO 1
 SF01 300.1618010 MHz
 NUC1 ^1H
 P0 4.67 usec
 P1 14.00 usec
 PLW1 7.62049998

F2 - Processing parameters
 SI 65536
 SF 300.1600078 MHz
 WDW EM
 SSB 0
 LB 0.30 Hz
 GB 0
 PC 1.00

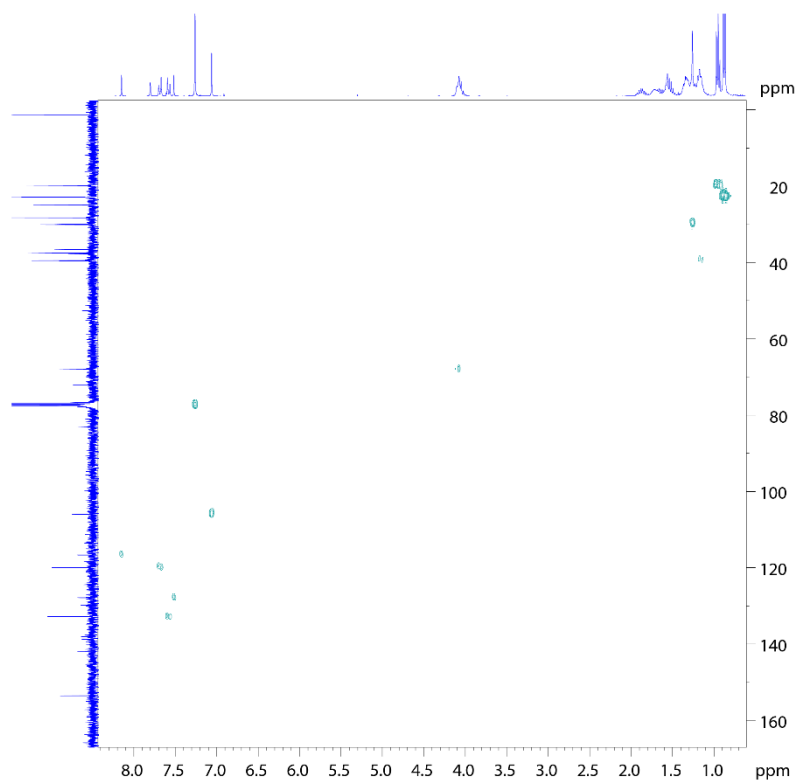


Current Data Parameters
NAME Q05YD255T
EXPNO 351
PROCNO 1

F2 - Acquisition Parameters
Date_ 20191106
Time h 3.36
INSTRUM spect
PROBHD Z104275_0303
PULPROG zgpg30
TD 65536
SOLVENT CDCl3
NS 800
DS 4
SWH 18115.941 Hz
FIDRES 0.552855 Hz
AQ 1.8087935 sec
RG 13.95
DW 27.600 usec
DE 6.50 usec
TE K 298.0
D1 2.00000000 sec
D11 0.03000000 sec
TD0 1
SF01 75.4835188 MHz
NUC1 13C
P0 3.33 usec
P1 10.00 usec
PLW1 40.0999847
SF02 300.1612006 MHz
NUC2 1H
CPDPRG2 waltz16
PCPD2 90.00 usec
PLW2 7.62049998
PLW12 0.18459000
PLW13 0.09284800



^{13}C NMR (CDCl_3 , 125 MHz, 298 K) of compound **1b**



^1H , ^{13}C -HMBC spectrum (CDCl_3 , 298 K) of compound **1b**

4. Supplementary Figures and Tables

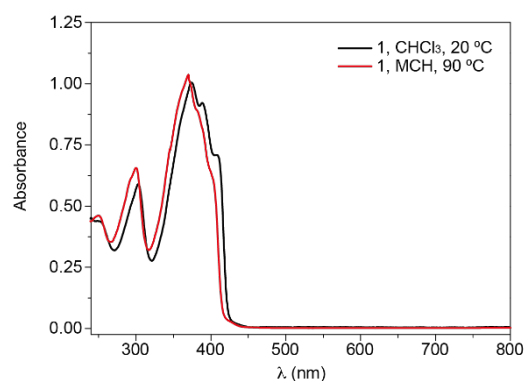


Figure S1. UV-Vis spectra of **1a** in CHCl_3 at 20 °C and MCH at 90 °C ($c_T = 10 \mu\text{M}$).

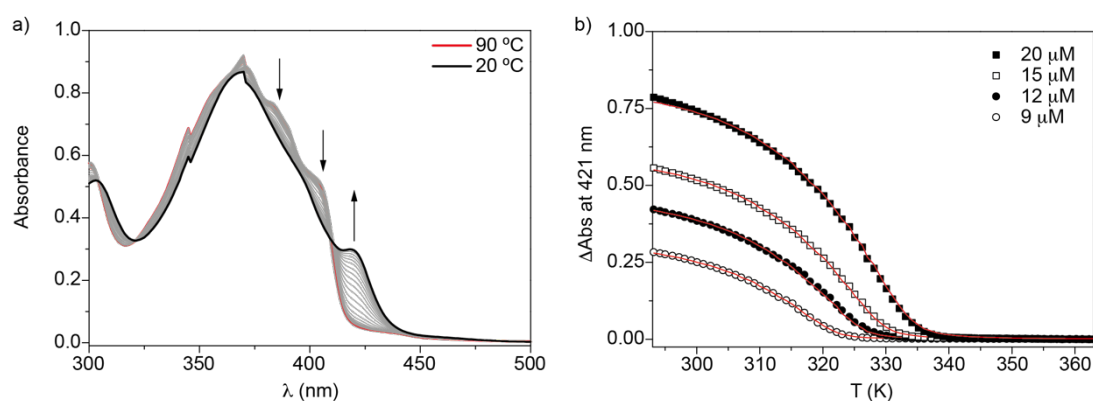


Figure S2. a) UV-Vis spectra of **1b** at different temperatures (MCH, $c_T = 12 \mu\text{M}$). Arrows indicate the changes in the absorption bands upon decreasing the temperature. b) Cooling curves (1 K min^{-1}) of **1b** in MCH at different concentrations. Red lines depict the fitting to the one-component EQ model.

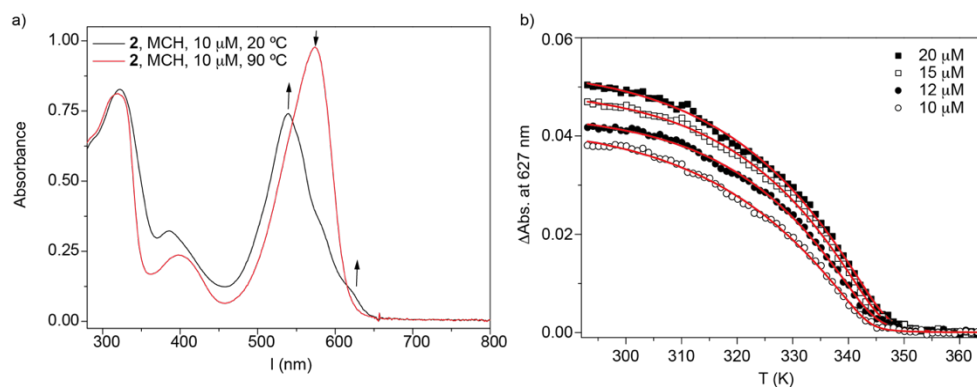


Figure S3. a) UV-Vis spectra of **2** at different temperatures (MCH, $c_T = 10 \mu\text{M}$). Arrows indicate the changes in the absorption bands upon decreasing the temperature. b) Cooling curves (1 K min^{-1}) of **2** in MCH at different concentrations. Red lines depict the fitting to the one-component EQ model.

Table S1. Thermodynamic parameters (nucleation enthalpy (ΔH_n), elongation enthalpy (ΔH_e), elongation entropy (ΔS), nucleation (K_n) and elongation (K_e) binding constants, and cooperativity factor (σ) inferred for compounds **1** and **2** in MCH as solvent.

	1a	1b	2
ΔH_e [kJ mol ⁻¹]	-43.6 ± 1	-54.8 ± 1	-47.3 ± 1
ΔS [J K ⁻¹ mol ⁻¹]	-35 ± 3	-74 ± 1	-44 ± 3
ΔH_n [kJ mol ⁻¹] ^a	-22.3 ± 3	-17.4 ± 1	-20.0 ± 3
σ ^a	1.3 × 10 ⁻⁴	7.7 × 10 ⁻⁴	2.6 × 10 ⁻⁴
K_e [L mol ⁻¹] ^a	8.8 × 10 ⁵	8.1 × 10 ⁵	1.4 × 10 ⁶
K_n [L mol ⁻¹] ^a	9.1 × 10 ¹	6.2 × 10 ²	3.6 × 10 ²
T_e [°C]	58, 62, 66, 69 ^b	48, 51, 55, 59 ^c	69, 71, 72, 73 ^d

[a] The equilibrium constants for elongation and dimerization, K_e and K_n , and the cooperativity factor σ ($= K_n / K_e$) are calculated at 298 K. ^bDerived at $c_T = 7, 10, 15$ and $20 \mu\text{M}$; ^cDerived at $c_T = 9, 12, 15$ and $20 \mu\text{M}$; ^dDerived at $c_T = 10, 12, 15$ and $20 \mu\text{M}$.

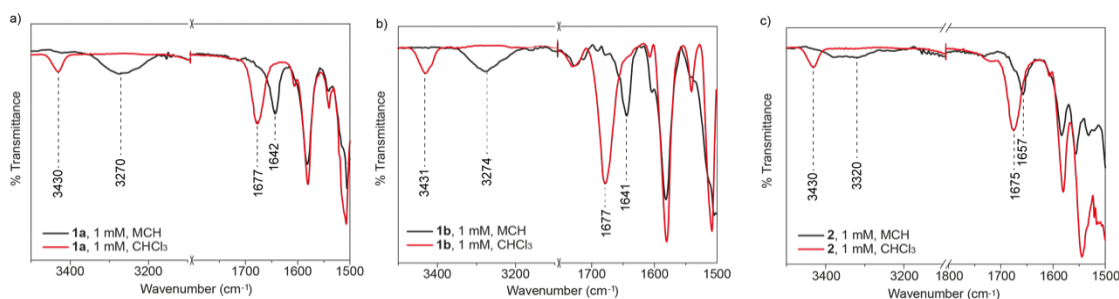


Figure S4. Partial FTIR spectra recorded for **1a** (a), **1b** (b), and **2** (c) in solution at $c_T = 1 \text{ mM}$ in MCH (black) and CHCl_3 (red) showing the region in which the stretching N-H and Amide I bands are observed.

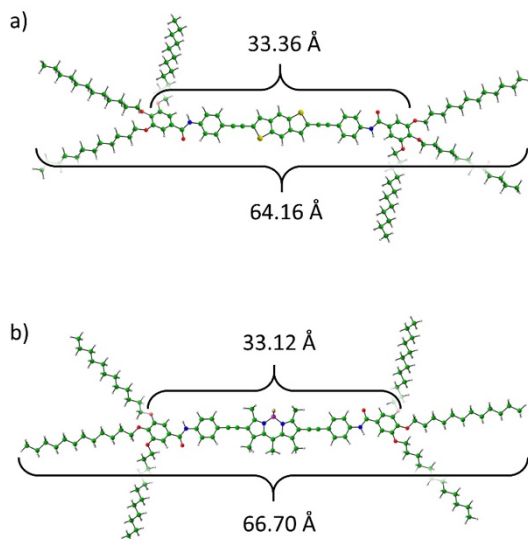


Figure S5. GFN2-xTB-optimized geometries calculated for the monomers of **1a** (a) and **2** (b). The lengths of the linear BDT- and BODIPY-based cores and of the whole molecules are indicated.

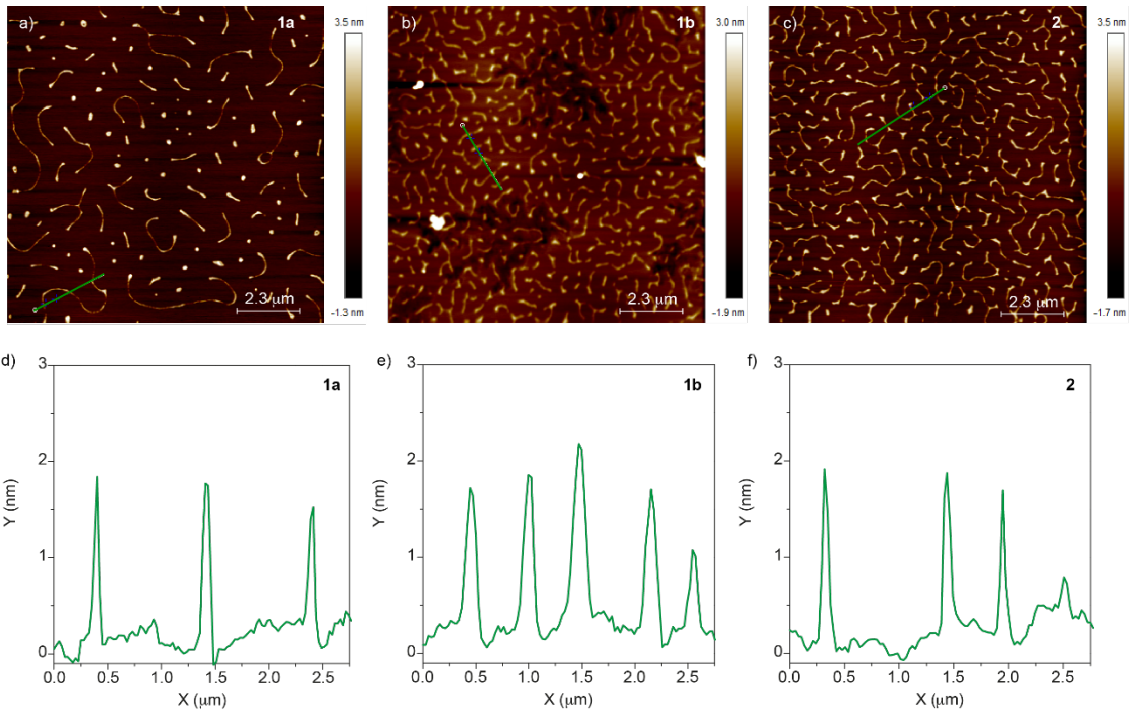


Figure S6. Height AFM images (a-c) and height profiles along the green line (d-f) of **1a** (a, d), **1b** (b, e), and **2** (c, f). Experimental conditions for AFM imaging: mica as surface; MCH, $c_T = 25 \mu\text{M}$, spin coating.

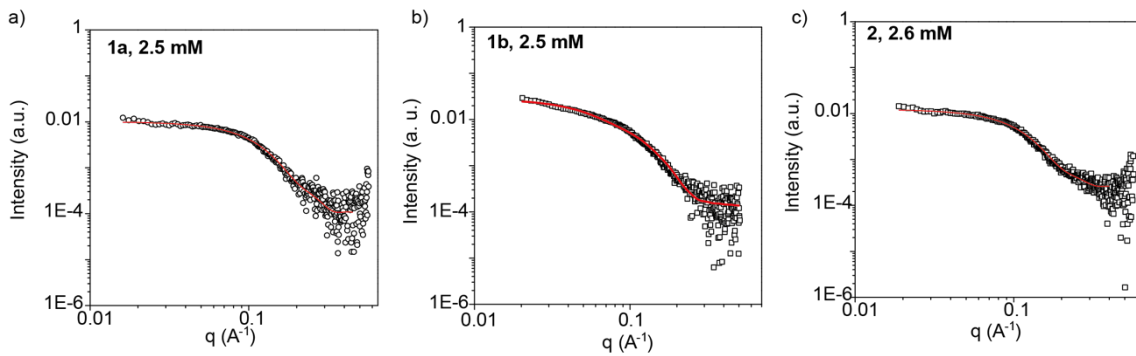


Figure S7. Experimental SAXS profiles (black symbols) for (a) **1a** (2.5 mM), (b) **1b** (2.5 mM), and (c) **2** (2.6 mM) in MCH, and the corresponding fitting curves (red lines) to the elliptical cylinder model.

Table S2. Fitting parameters to the elliptical cylinder model of the experimental SAXS profiles of **1**, **2**, and **1-co-2** supramolecular aggregates in MCH at different concentrations.

	c_T (mM) / (mg/mL)	r^a (Å)	r error (Å)	Axis Ratio ^b	Length/ (Å)	Length error (Å)	χ^2
1a	1 / 1.7	10.45	0.27	2.1	37	4	1.42
1a	2.5 / 4.3	10.05	0.22	2.2	37	5	1.52
1b	1.05 / 1.6	10.54	0.75	1.7	123	5	0.90
1b	2.6 / 4.1	11.21	0.27	1.6	95	1	2.44
2	1 / 1.8	9.80	0.23	2.2	43	2	0.91
2	2.6 / 4.7	10.74	0.32	2.1	38	5	1.52
1a-co-2	1 / 1.8	10.43	0.28	2.1	37	5	1.22
1a-co-2	3.3 / 5.8	10.82	0.21	1.9	36	3	1.53
1b-co-2	1 / 1.7	9.51	0.80	1.8	64	2	1.26
1b-co-2	2.5 / 4.2	9.37	0.30	2.0	47	1	1.17

^a " r " corresponds to the minor radius. ^b The axis ratio indicates the relation between the minor and major radius.

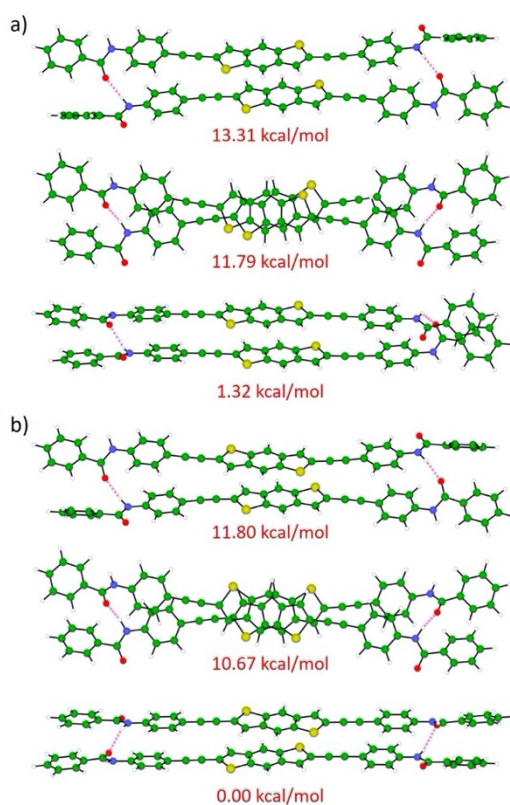


Figure S8. Minimum-energy structures calculated at the GFN2-xTB level for the different possible conformations of a BDT dimer of **1** in a parallel (a) and an antiparallel (b) stacking arrangement, based on the intermolecular H-bonding (from top to bottom: lineal, helical, and weakly directional). Relative energies with respect to the most stable conformer are indicated.

Table S3. Relative energies calculated at the B3LYP-D3/6-31G(d,p) level of theory for the different possible conformations of the BDT dimer of **1** sketched in Figure S8.

Conformer	E_{rel} (kcal mol ⁻¹)
lineal parallel	13.40
helical parallel	12.09
weakly directional parallel	1.04
lineal antiparallel	12.73
helical antiparallel	11.40
weakly directional antiparallel	0.00

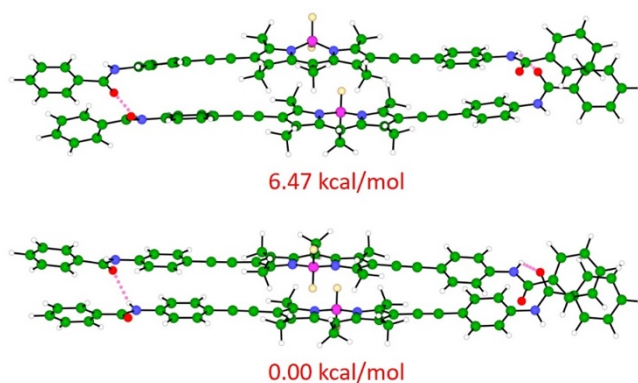


Figure S9. Minimum-energy structures calculated at the GFN2-xTB level for the parallel (top) and antiparallel (bottom) stacking arrangements in the BODIPY dimer of **2**. Relative energies with respect to the most stable conformer are indicated.

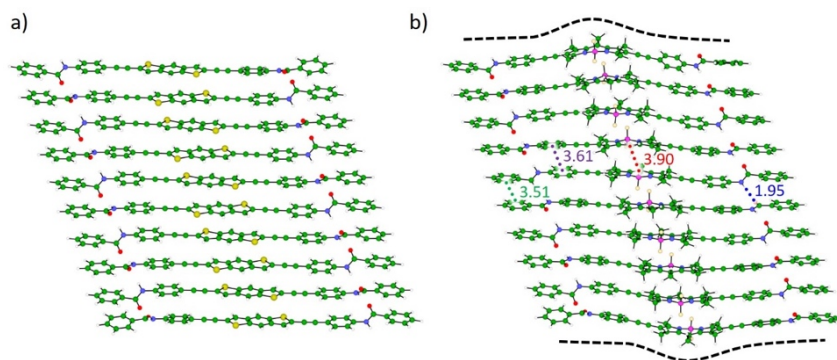


Figure S10. Minimum-energy structures calculated at the GFN2-xTB level for a decamer stacking of BDT **1** (a) and BODIPY **2** (b) without peripheral aliphatic chains. Relevant intermolecular mean distances (in Å) calculated for the decamer are indicated in (b).

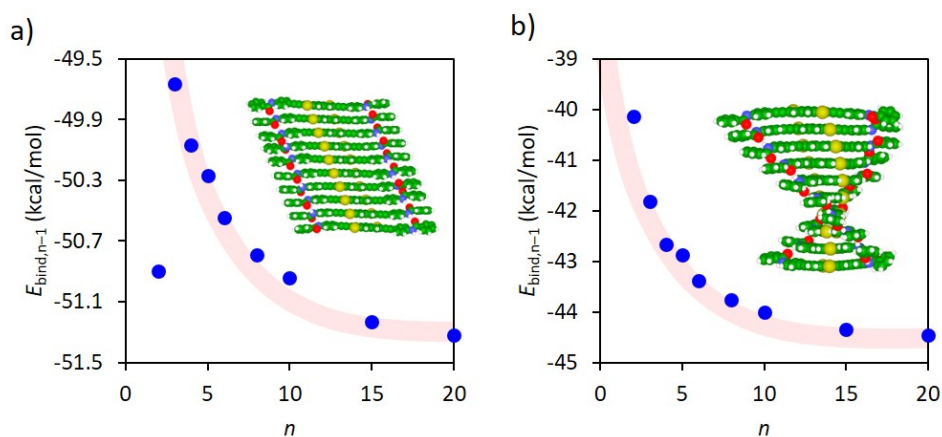


Figure S11. Evolution of the binding energy per interacting pair as a function of the number of monomers (n) calculated at the GFN2-xTB level for slipped (a) and helical (b) supramolecular assemblies of BDT **1** (without peripheral aliphatic chains) with a parallel stacking of the core. Transparent red lines are drawn to guide the eye.

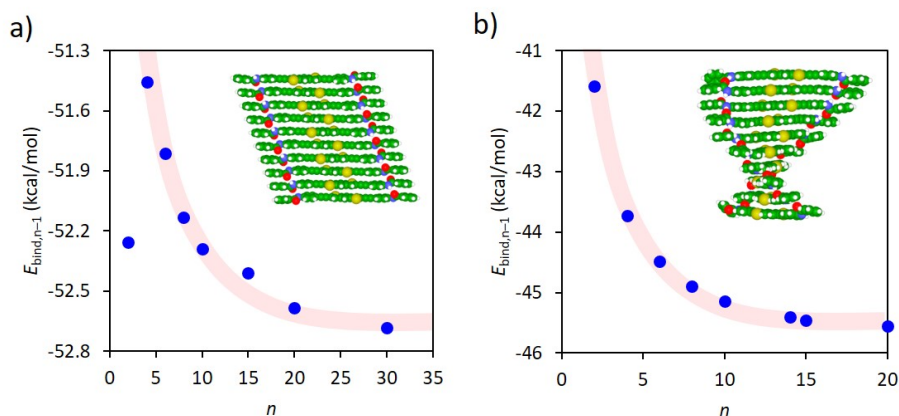


Figure S12. Evolution of the binding energy $E_{\text{bind},n-1}$ as a function of the number of monomers (n) calculated at the GFN2-xTB level for slipped (a) and helical (b) supramolecular assemblies of BDT **1** (without peripheral aliphatic chains) with an antiparallel stacking of the core. Transparent red lines are drawn to guide the eye.

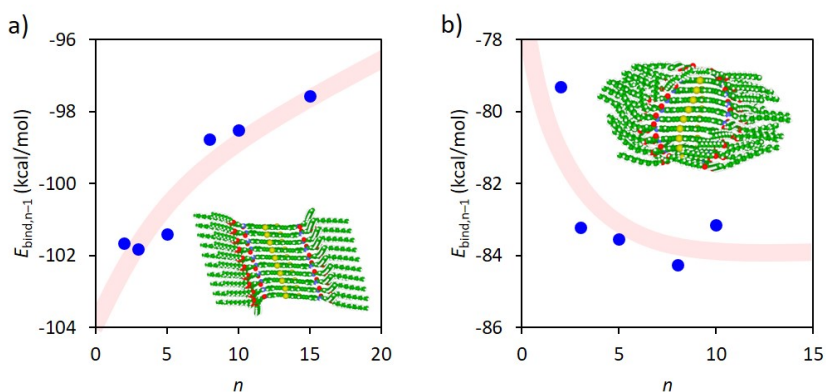


Figure S13. Evolution of the binding energy per interacting pair as a function of the number of monomers (n) calculated at the GFN2-xTB level for slipped (a) and helical (b) supramolecular assemblies of BDT **1** (with peripheral aliphatic chains) with a parallel stacking of the core. Transparent red lines are drawn to guide the eye.

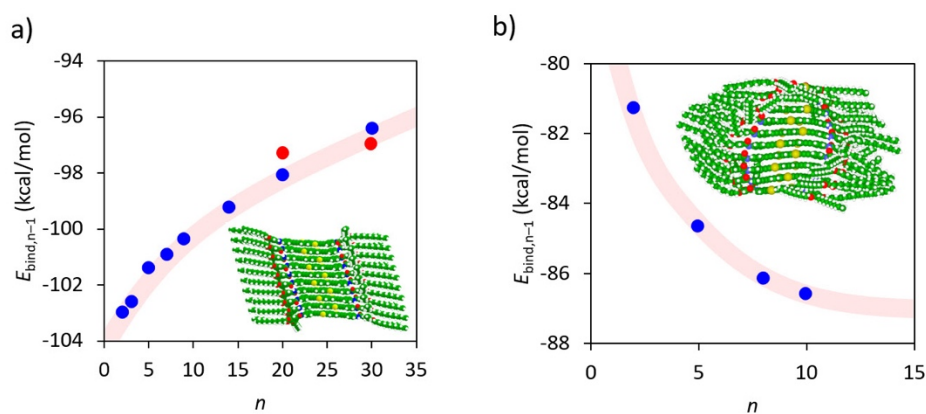


Figure S14. Evolution of the binding energy per interacting pair as a function of the number of monomers (n) calculated at the GFN2-xTB level for slipped (a) and helical (b) supramolecular assemblies of BDT **1** (with peripheral aliphatic chains) with an antiparallel stacking of the core. Transparent red lines are drawn to guide the eye.

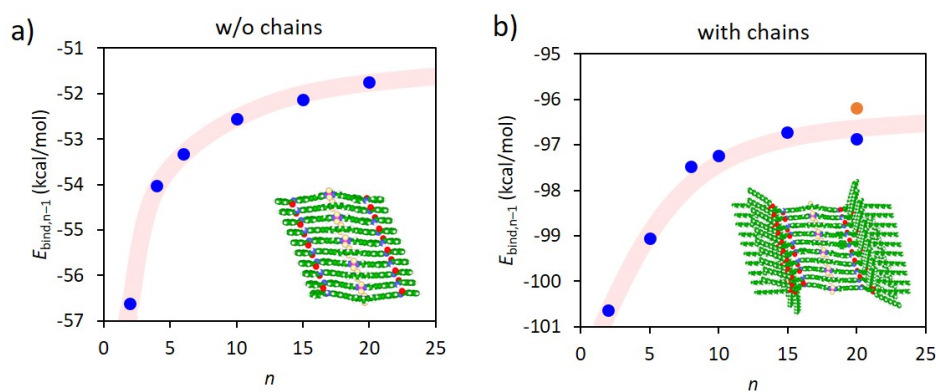


Figure S15. Evolution of the binding energy per interacting pair as a function of the number of monomers (n) calculated at the GFN2-xTB level for the most stable arrangement of BODIPY **2** without (a) and with (b) peripheral aliphatic chains. The orange point in (b) corresponds to a central-distorted 20-mer (see Figure S15b). Transparent red lines are drawn to guide the eye.

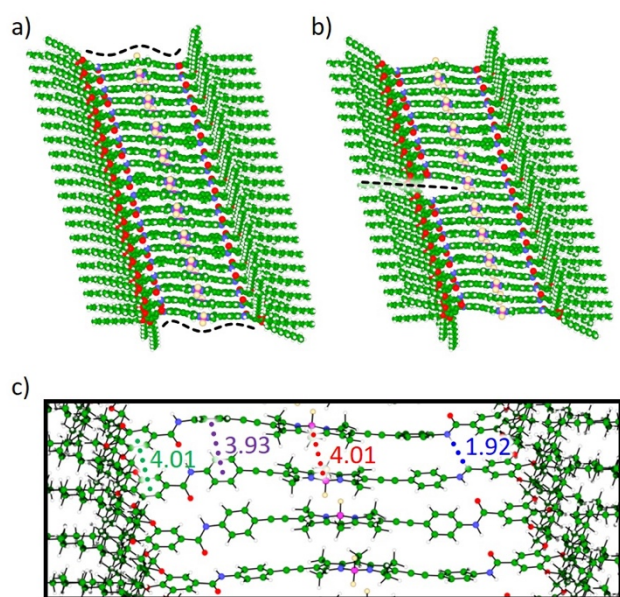


Figure S16. Minimum-energy structures calculated at the GFN2-xTB level for a fully-interacting (a) and a central-disrupted (b) 20-mer of BODIPY **2**. c) Relevant intermolecular mean distances (in Å) calculated for a decamer of **2** bearing the long peripheral aliphatic chains.

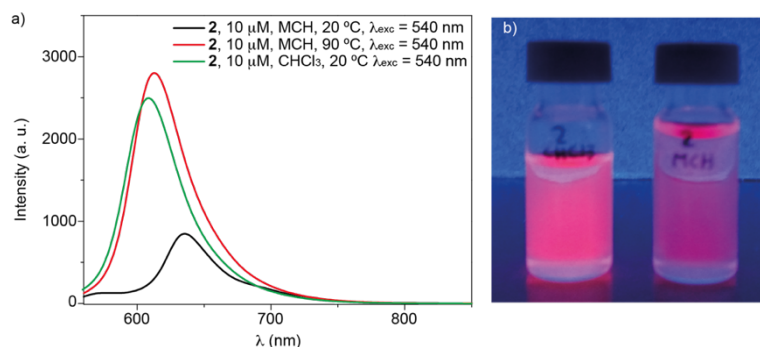


Figure S17. a) Fluorescence spectra of compound **2** at different temperatures and solvents. b) Pictures of the emissive solutions of **2** in CHCl_3 (left) and MCH (right) at 20 °C under UV-light irradiation at $\lambda_{\text{exc}} = 364 \text{ nm}$ ($c_T = 10 \mu\text{M}$).

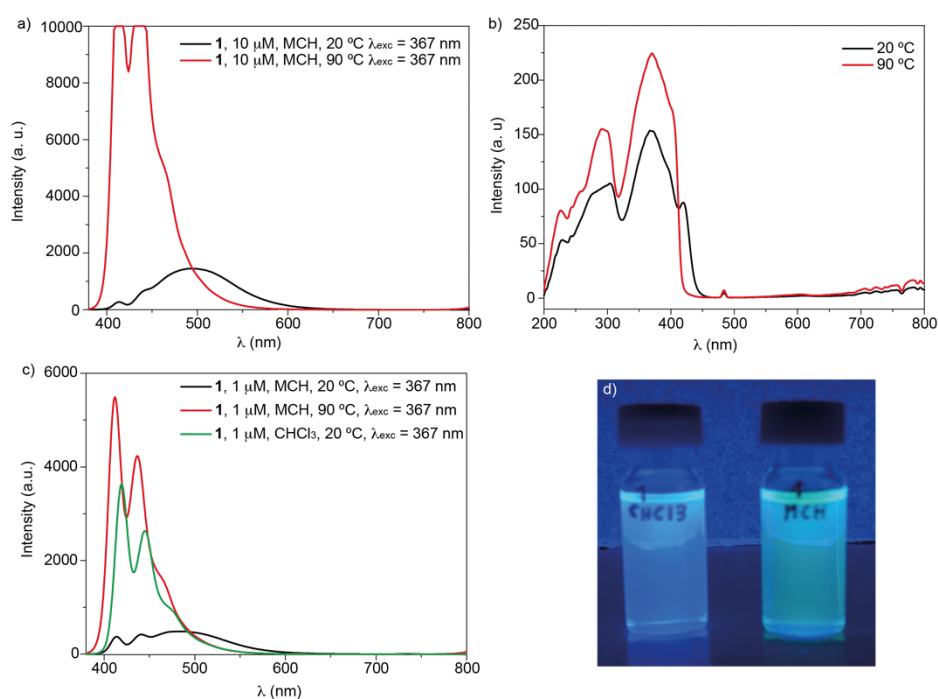


Figure S18. a, b, c) Fluorescence (a,c) and excitation (b) spectra of compound **1a** at different temperatures, concentrations, and solvents. c) Pictures of emissive solutions of **1** in CHCl_3 (left) and MCH (right) at 20 °C under UV-light irradiation at $\lambda_{\text{exc}} = 364 \text{ nm}$ ($c_T = 10 \mu\text{M}$).

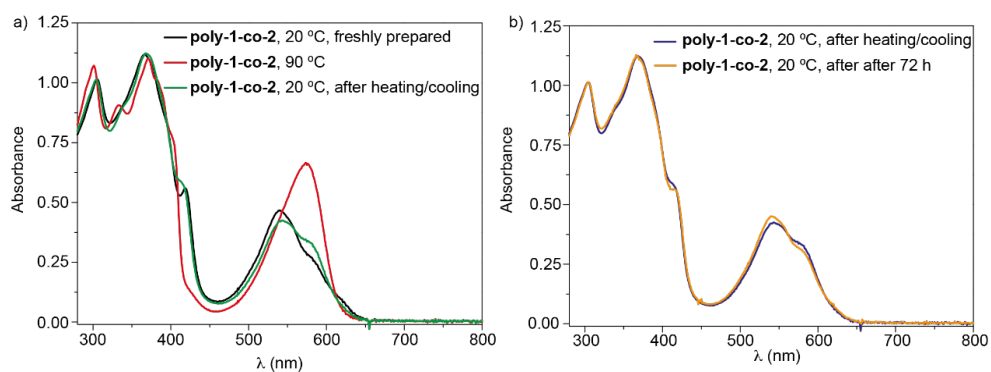


Figure S19. UV-Vis spectra of an equimolar mixture of **1a** and **2** at different experimental conditions of temperature and time using MCH as solvent ($c_T = 10 \mu\text{M}$).

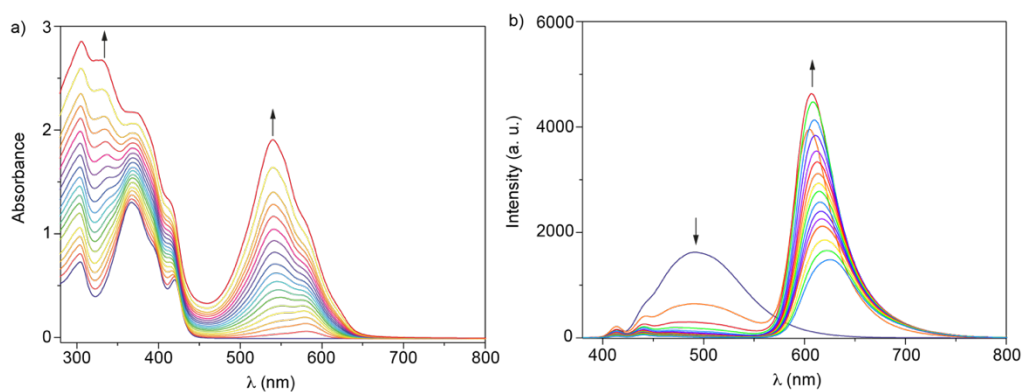


Figure S20. UV-Vis (a) and emission (b) spectra of mixtures of **1a** and **2** at different ratios in MCH at $20 \text{ }^\circ\text{C}$ ($c_T = 20 \mu\text{M}$; $\lambda_{\text{exc}} = 367 \text{ nm}$). Arrows indicate the changes in the absorption and emission bands upon increasing the amount of BODIPY **2**.

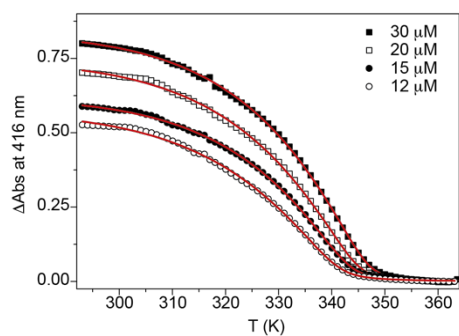


Figure S21. Plot of the variation of the absorbance at $\lambda = 595 \text{ nm}$ versus temperature cooling at 1 K min^{-1} for **1a-co-2**. Red curves correspond to the global fitting to the EQ model to guide the eye.

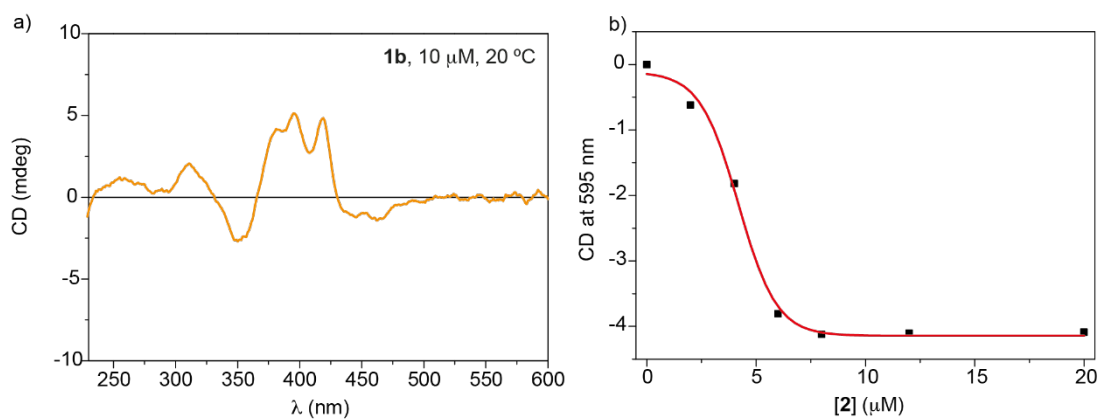


Figure S22. (a) CD spectrum of **1b** in MCH. (b) Plot of the variation of the dichroic response at $\lambda = 595$ nm in mixtures of **1b** and **2** upon increasing the amount of added **2** (MCH, $c_T = 10$ μ M, 20 $^{\circ}$ C). The red line in panel (b) corresponds to a Boltzmann fit to guide the eye.

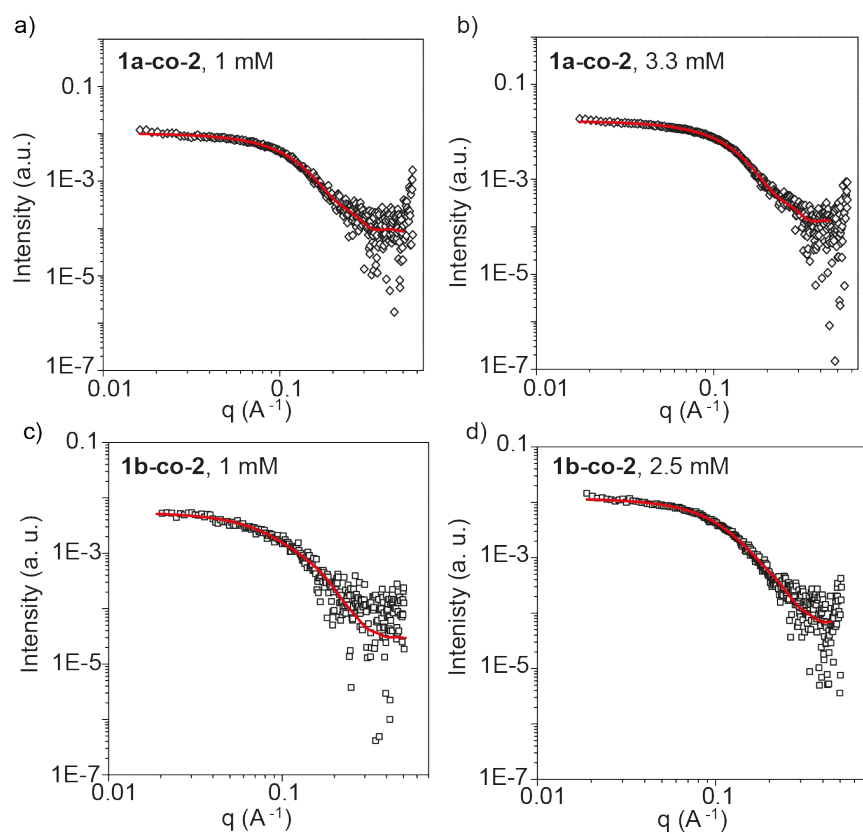


Figure S23. SAXS data and fitting for **1a-co-2** (a, b) and **1b-co-2** (c, d) at 1 mM (a, c), 3.3 mM (b) and 2.5 mM (d) in MCH. The red lines depict the fitting to the elliptical cylinder mode.

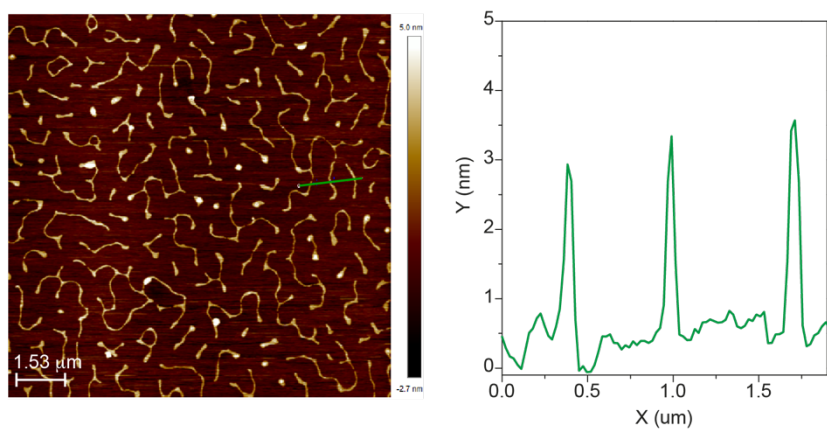


Figure S24. Height AFM image (a) and height profile along the green line (b) of **1a-co-2**. Experimental conditions for AFM imaging: mica as surface; MCH, $c_T = 25 \mu\text{M}$, spin coating.

5. SAXS measurements

For compounds **1a**, **1b**, and **2**, the solid compound was dissolved in the appropriate amount of MCH ($c_T = 1$ or 2.5 mM), heated to 90° for 2 minutes, and then allowed to cool and stabilize at room temperature for 24 h prior to the measurements. The samples of the co-assembled species (**1a-co-2** and **1b-co-2**) were prepared by mixing, at 1:1 ratio, CHCl_3 solutions of **1a** or **1b** and **2** ($c_T = 1$ mM) and then evaporating the solvent under argon flow. The resulting solid was re-dissolved in the appropriate amount of MCH and the sample was allowed to stabilize for 24 h prior to the measurements.

Background subtraction (against the solvent) was carried out using the XSACT software (Xenocs). The subtracted curves were fitted to customized models using the software SASView. The curves were fitted to distinct models and the best fittings (χ^2) for the SAXS curves of the **1**, **2**, and **1-co-2** supramolecular aggregates were obtained using the elliptical cylinder model (Table S2).

5. Theoretical calculations

Theoretical calculations were performed by means of the xTB program package.^{S2} Full geometry optimizations were carried out at the cost-effective semiempirical GFN2-xTB level of theory, which uses a minimal valence basis set centred on atoms (STO-mG), and includes the latest density-dependent D4 dispersion correction.^{S3} Figures S5 and S8-S16 show the optimized geometries computed for monomers and for aggregates of increasing size (from the dimer to the 30-mer). The binding energy per interacting pair ($\Delta E_{\text{bind},n-1}$) was calculated as:

$$\Delta E_{\text{bind},n-1} = \frac{E_{\text{oligomer}} - nE_{\text{monomer}}}{n-1}$$

where E_{oligomer} is the energy for a specific oligomer, E_{monomer} is the energy for the minimum-energy geometry of the corresponding monomer, and n is the number of monomeric units in the oligomer. Figures S11-S14 and Figure 5b,c in the main text show the evaluation of $\Delta E_{\text{bind},n-1}$ with the size of the oligomer. Central-disrupted oligomers were built up by joining two optimized decamers, and then fully optimizing at the GFN2-xTB level (Figure S16b and Figure 6b).

Solvent effects were included to assess dimer stability of BDT **1** by means of the generalized Born (GB) model with surface area (SA) contributions (termed GBSA approach). The relative energies calculated at the GFN2-xTB+GBSA level for the helical stacking arrangement with respect to the most stable cofacial, slightly long-axis slipped, antiparallel conformer in a BDT dimer of **1** were calculated to be 10.67, 5.14, 4.62, and 4.38 kcal mol⁻¹ in vacuum, *n*-hexane, chloroform, and toluene, respectively, thus confirming the higher energy of the helical dimer. Density functional theory calculations were also performed on the different conformations of the dimeric species of BDT **1** through the Gaussian-16.A03 suite of programs.^{S4} Geometry optimizations and single-point energy calculations were carried out by means of the popular hybrid B3LYP functional^{S5} and the double-zeta Pople's 6-31G(d,p) basis set, and including the Grimme's D3 dispersion correction.^{S6,S7} Relative energies are summarized in Table S2.

Geometry representations and analyses were done by means of the Chemcraft 1.7 software.^{S8}

References

- [S1] (a) A. Rödle, B. Ritschel, C. Mück-Lichtenfeld, V. Stepanenko, G. Fernández, *Chem. Eur. J.* **2016**, *22*, 15772–15777; (b) F. Wang, M. A. J. Gillissen, P. J. M. Stals, A. R. A. Palmans, E. W. Meijer, *Chem. Eur. J.* **2012**, *18*, 11761–11770
- [S2] C. Bannwarth, E. Caldeweyher, S. Ehlert, A. Hansen, P. Pracht, J. Seibert, S. Spicher, S. Grimme, *WIREs Comput. Mol. Sci.*, **2020**, *11*, e01493.
- [S3] C. Bannwarth, S. Ehlert, S. Grimme, *J. Chem. Theory Comput.* **2019**, *15*, 1652–1671.
- [S4] Gaussian 16, Revision A.03, M. J. Frisch, G. W. Trucks, H. B. Schlegel, G. E. Scuseria, M. A. Robb, J. R. Cheeseman, G. Scalmani, V. Barone, G. A. Petersson, H. Nakatsuji, X. Li, M. Caricato, A. V. Marenich, J. Bloino, B. G. Janesko, R. Gomperts, B. Mennucci, H. P. Hratchian, J. V. Ortiz, A. F. Izmaylov, J. L. Sonnenberg, D. Williams-Young, F. Ding, F. Lipparini, F. Egidi, J. Goings, B. Peng, A. Petrone, T. Henderson, D. Ranasinghe, V. G. Zakrzewski, J. Gao, N. Rega, G. Zheng, W. Liang, M. Hada, M. Ehara, K. Toyota, R. Fukuda, J. Hasegawa, M. Ishida, T. Nakajima, Y. Honda, O. Kitao, H. Nakai, T. Vreven, K. Throssell, J. A. Montgomery, Jr., J. E. Peralta, F. Ogliaro, M. J. Bearpark, J. J. Heyd, E. N. Brothers, K. N. Kudin, V. N. Staroverov, T. A. Keith, R. Kobayashi, J. Normand, K. Raghavachari, A. P. Rendell, J. C. Burant, S. S. Iyengar, J. Tomasi, M. Cossi, J. M. Millam, M. Klene, C. Adamo, R. Cammi, J. W. Ochterski, R. L. Martin, K. Morokuma, O. Farkas, J. B. Foresman, and D. J. Fox, Gaussian, Inc., Wallingford CT, **2016**.
- [S5] A. D. Becke, *J. Chem. Phys.* **1993**, *98*, 5648–5652.
- [S6] V. A. Rassolov, M. A. Ratner, J. A. Pople, P. C. Redfern, L. A. Curtiss, *J. Comp. Chem.* **2001**, *22*, 976–984.
- [S7] S. Grimme, S. Ehrlich, L. Goerigk, *J. Comp. Chem.* **2011**, *32*, 1456–1465.
- [S8] Chemcraft - graphical software for visualization of quantum chemistry computations. <https://www.chemcraftprog.com>.